



Article

Autonomous Wireless Sensor Networks in an IPM Spatial Decision Support System[†]

Mina Petrić^{1,2,3,*} , Jurgen Vandendriessche^{4,5}, Cedric Marsboom¹, Tom Matheussen¹, Els Ducheyne¹ and Abdellah Touhafi^{4,5}

¹ Avia-GIS NV, 2980 Zoersel, Belgium; cmarsboom@avia-gis.com (C.M.); tmatheussen@avia-gis.com (T.M.); elseducheyne@gmail.com (E.D.)

² Department of Physics and Astronomy, Faculty of Sciences, University of Gent, 9000 Gent, Belgium

³ Department of Physics, Faculty of Sciences, University of Novi Sad, 21000 Novi Sad, Serbia

⁴ Department of Electronics and Informatics, Vrije Universiteit Brussels, 1050 Ixelles, Belgium; jurgen.vandendriessche@vub.be (J.V.); abdellah.touhafi@vub.be (A.T.)

⁵ Lumency bvba, 1020 Brussels, Belgium

* Correspondence: mpetric@avia-gis.com

[†] This paper is an extended version of our paper published in: Petrić, M.; Marsboom, C.; Matheussen, T.; Ducheyne, E.; Vandendriessche, J.; Touhafi, A. Autonomous Wireless Sensor Networks in automated IPM (CloudTech 2018), Brussels, Belgium, 26–28 November 2018.

Received: 15 April 2019; Accepted: 23 May 2019; Published: 28 May 2019



Abstract: Until recently data acquisition in integrated pest management (IPM) relied on manual collection of both pest and environmental data. Autonomous wireless sensor networks (WSN) are providing a way forward by reducing the need for manual offload and maintenance; however, there is still a significant gap in pest management using WSN with most applications failing to provide a low-cost, autonomous monitoring system that can operate in remote areas. In this study, we investigate the feasibility of implementing a reliable, fully independent, low-power WSN that will provide high-resolution, near-real-time input to a spatial decision support system (SDSS), capturing the small-scale heterogeneity needed for intelligent IPM. The WSN hosts a dual-uplink taking advantage of both satellite and terrestrial communication. A set of tests were conducted to assess metrics such as signal strength, data transmission and bandwidth of the SatCom module as well as mesh configuration, energetic autonomy, point to point communication and data loss of the WSN nodes. Finally, we demonstrate the SDSS output from two vector models forced by WSN data from a field site in Belgium. We believe that this system can be a cost-effective solution for intelligent IPM in remote areas where there is no reliable terrestrial connection.

Keywords: wireless sensor networks; integrated pest management; spatial decision support system; LoRa; satellite communication; *Aedes albopictus*

1. Introduction

Pest monitoring and control is becoming an increasingly important issue worldwide, with invasive pest species seizing the spotlight and adapting to new environments at an alarming rate. This is supported by the impact of climate change turning previously unsuitable areas to current and future hotspots for invasive species and emerging infectious disease. The main threat of invasive species is their ability to vector a wide array of diseases. The World Health Organisation (WHO) estimates that vector-borne diseases account for more than 17% of all infectious diseases, with more than 9.8 billion people at risk, 96 million reported cases, and over 700 thousand deaths annually [1]. Efficient local monitoring or surveillance is essential to prevent the spread and establishment of pests, especially in ports, warehouses with imported plants, stockpiles of tires, rest areas on highways and

train stations. The European Centre for Disease Control (ECDC), the European Environment Agency (EEA), and health/environmental protection agencies in all EU member states are responsible for the implementation of mosquito surveillance programmes. There are still many regions in Europe without any kind of mosquito surveillance programmed being implemented, but this is rapidly changing due to the threat of climate change.

The role of precise in situ sensor data, as well as Earth Observation (EO), is manifold. Remote sensed data can provide information for determining ecoclimatic zones with different levels of environmental suitability for the pest and precise WSN data can drive intelligent dynamical population models to target peaks in the pest population and inform control action, limiting the harmful effect on the environment from the excessive application of pesticides.

Sensor networks are already widely used in many urban and suburban settings. This number will only increase given the rise of “Internet of Things” (IoT). According to Gardner there are already more connected “things” than people in the world. The number of devices in the IoT network is expected to reach 20.4 billion by 2020 [2]. Accordingly, there have already been a number of studies to monitor and control pests using WSN technologies. However, there is still a considerable gap in pest management using WSN with most current applications failing to provide a low-cost, self-sufficient monitoring system that can operate in remote areas. A lot of the existing systems rely on the availability of a power grid and WiFi or a cellular communication network. This is not a problem in urban areas however, pest management requires surveillance in remote areas where a local network and power supply are not present, and the dependency on terrestrial networks is untrustworthy.

In addition to the lack of coverage, communication reliability and data acquisition and processing delays are also a significant consideration. Until recently, data acquisition in integrated pest management (IPM) relied on manual collection of pest and meteorological data. This is tedious and cumbersome and incompatible with the models being developed to assist pest monitoring mainly because of the lag created by manual collection and processing. These models rely on NRT (near-real-time), subdaily environmental parameters to create the forcing fields necessary for computation. Satellite communication could provide a solution to the limitations of current systems and an uninterrupted NRT forcing for pest population dynamics forecast models.

Although local and cellular networks are widespread and commonly used, the spatial distribution is not homogenized around the world. They are mostly concentrated around major population hotspots. Large gaps in the spatial coverage of cellular networks do exist. This makes it hard to conduct automatic surveying and monitoring in remote locations.

Another reason in favor of using multiple communication modules within a single WSN is redundancy in case of weather interference. Cloud cover and precipitation can significantly affect the availability in the SatCom link. The attenuation of the uplink and downlink signals due to rain depend on the precipitation rate as well as the droplet size relative to the frequency of the satellite communication band, with the degradation increasing with frequency. The principal effect behind this is the attenuation of electromagnetic radiation passing through a liquid water medium. The highest attenuation occurs at the Ku-band (downlink frequency 12 GHz) which corresponds to the wavelength of 25 mm, while the lowest attenuation occurs for the C-band frequency (downlink 4 GHz) with the wavelength of 75 mm [3]. The closer the wavelength is to the diameter of the raindrop, which averages around 5 mm, the higher the attenuation of the incoming electromagnetic radiation. With 10/10 cloud cover and precipitation present, the SatCom link will be unavailable. On the other hand, the terrestrial link, while also experiencing attenuation, does so in a lesser manner with GSM frequency bands spanning from 380–900 MHz [4].

To secure reliable data feeding into IPM spatial decision support systems we have developed the PentaSense WSN framework, which, coupled with EO at different spatial scales feeds into numerical models. The gateway is constructed with a dual-uplink module integrating both terrestrial and satellite communication. This creates the possibility to implement a back-up system where both options are

available to increase reliability further and minimize operating costs. Moreover, embedded energy scavenging techniques can ensure long battery life.

The aim of this research is not to replace the terrestrial communication strategy but to provide a dual mode on the gateway to accommodate the highest degree of technological flexibility, especially for implementations that need to be accommodating to different pest environments worldwide. This will allow the smart traps and sensors to operate even when the terrestrial systems are or become unavailable. Adding satellite communications on the gateway also allows for easier system deployment. Where using local 2G/3G/4G networks requires contracts with local providers which need to be closed in each country of operation, satellite communication allows operating everywhere on the globe under the same contract and provider. This can be a very useful feature for prospecting operations and pilot studies.

Hence, in the PentaSense system the satellite communication is used a second communication link ensuring reliable, uninterrupted data transfer and redundancy for IPM applications. The dual-uplink can provide safe, cost-effective and secure communication even in areas where existing connections are overloaded, destroyed or not present. Moreover, this setup can provide a reliable transfer of payload meteorological data to the remote server in NRT regardless of the deployment location of the WSN.

Impact on Integrated Pest Management

During the last decade, there was a significant shift in pest control towards integrated pest management (IPM) approaches and practices. The implementation of many mechanistic pest population dynamics models, as well as disease model which directly build on the previous, enables us to apply intelligent, eco-friendly control measures before the pest achieves a significant density.

Wireless networks deployed to sense the micrometeorological variables of the environment of the pest coupled with earth observation products such as MODIS [5] and Sentinel [6] form the basis of the input fields driving these population and disease models.

Very high-resolution satellite images have been used to a limited extent as a means to determine habitat of insects in general [7] and disease vectors more specifically. De Roeck et al. [8], for example, used EO to determine the habitat of the vector of liver fluke, *F. hepatica* in Flanders, with a spatial resolution of 0.5 m. Mairota et al. [9] assessed at multiple scales the required grain for pest habitat detection. Datir et al. [10] demonstrate the application of a real-time system for the detection of the Downy Mildew pest. Srivastav et al. [11] developed a WSN alarm system based on the noise level generated by the pest; similarly, Srinivas [12] and Al-Manie et al. [13] look at acoustic levels for larvae, and pests inside infected date palm trees, respectively. An overview of is given in Azfar et al. [14])

There are many IPM applications available online in the form of internet-based information delivery systems [15]. Although most applications are in the form of static data repositories, there are also dynamical IPM tools that use weather and climate data as input to GDD (Growing degree-day) models [16,17], sampling cost calculator [18], as well as more complex phenology and pest population dynamics models [19]. Some authors suggest that SDSS systems could quickly become an absolute requirement for local, regional as well as international implementations of IPM surveillance and management programs [15,20]. Ambient temperature has the most significant impact on mortality and development rates for the majority of pest species; however, other abiotic factors such as precipitation, relative humidity, soil moisture, wind speed and level of urbanization, as well as biotic parameters such as density-dependent mortality can have an influence on the population dynamics [20–22].

The potential for very high-resolution EO features to be used for measuring and monitoring habitat quality and biodiversity is confirmed, yet important scaling issues exist and must be taken into consideration. The computational costs involved in the choice of different computational scales for textural high-resolution EO features are substantial as computational time increases exponentially with increasing window size. This is especially relevant for insects where very high resolution is required.

WSNs can provide in situ, high resolution, NRT monitoring of the processes essential to the pest life cycle in the zones outlined by EO analysis. The data collection and network design should

be driven by the following requirements: (a) Measurement fidelity; (b) Sampling frequency: ideally measurements should be taken every 3 min and optimally every min; (c) Accuracy, precision and range: preferably, the sensor accuracy should not be less than: $<\pm 0.5$ °C for air temperature; $<\pm 5\%$ for relative humidity and $<\pm 4\%$ for precipitation. The operation range for the temperature sensor should be -20 to $+70$ °C; (d) A sustainable power supply for long-term field operation: The low power aspect of WSNs can allow for exploring energy-efficient options that would eliminate the requirement for a battery on the sensory nodes such as embedded energy harvesting with supercapacitors; and (e) Harsh environment and enclosure: To ensure reliable data collection over longer periods, both the node hardware and sensors must perform well under harsh conditions.

Basic data cleaning and aggregation algorithms need to be employed to generate forcing for all the sites in parallel and combine on different scales. Quality Control (QC) of the incoming data must be done in near-real time or shortly after the measurements to minimize data loss and shorten the time to identify and fix problems.

Pest population dynamics are driven by environmental factors at the global and local scale. The El Niño/Southern Oscillation Index (ENSO), for example, is a global phenomenon with an impact on human infectious disease risk worldwide through droughts, flood, and other weather extremes [23–26]. On the other side of the time spectrum, locally measured rainfall/temperature with very high temporal frequency will also drive the population dynamics more directly [27,28]. Capturing the micro-meteorological conditions that are specific to pest resting sites could significantly increase the accuracy of currently used population dynamics models as well as disease transmission models since the processes pertaining to disease incubation rates are also temperature dependent [29].

In this paper, we examine the application of the “PentaSense” wireless network on a specific vector, *Ae. albopictus*, best known as the Asian tiger mosquito. It was first introduced in Europe around the end of the 20th century and has since spread to most of the countries on the continent. This mosquito has vector competence for a wide range of disease such as Dengue, Yellow fever, Chikungunya and Zika [30–33].

The main environmental factors influencing the establishment of this mosquito and driving the inter-annual population dynamics are temperature and precipitation. Climate normals and long-term averages can be used to describe the niche regional suitability for the establishment of the vector, however daily and sub-daily values of the meteorological variables are needed to drive the population dynamics. Autonomous Wireless Sensor Networks (WSN) can provide precise, site-specific information of the most important variables in remote areas and allow us to model the vector population.

The paper describes the developed WSN-SDSS framework and the results of two model applications for the simulation of climatic suitability and micro-meteorological driven dynamics of *Ae. albopictus*.

2. Materials and Methods

2.1. The PentaSense Network

The ground sensors form a WSN with a smart gateway, surrounded by modular, multi-sensor nodes in a multi-hop mesh. The complete system is divided into three semi-independent parts, the PentaSense WSN, the communication module and the SDSS (spatial decision support system) which will aggregate WSN sensor and meta-data with EO on a remote server. Each multi-sensor node communicates the collected data to the central sink node or the gateway. The gateway is equipped with a two-way communication system integrating a satellite module and terrestrial communication. In addition, finally, the SDSS is designed to store the data in a local database, and to analyze and display the information in an easy to interpret way for the user through a web application. Overview of the system architecture is shown in Figure 1.

The design of the communication framework considers aspects like end-to-end reliability, expected network lifetime and existing infrastructure, etc. A power-independent WSN designs that provides low-power, low-cost and reduced data rate wireless transmissions either in mesh networks is evaluated.

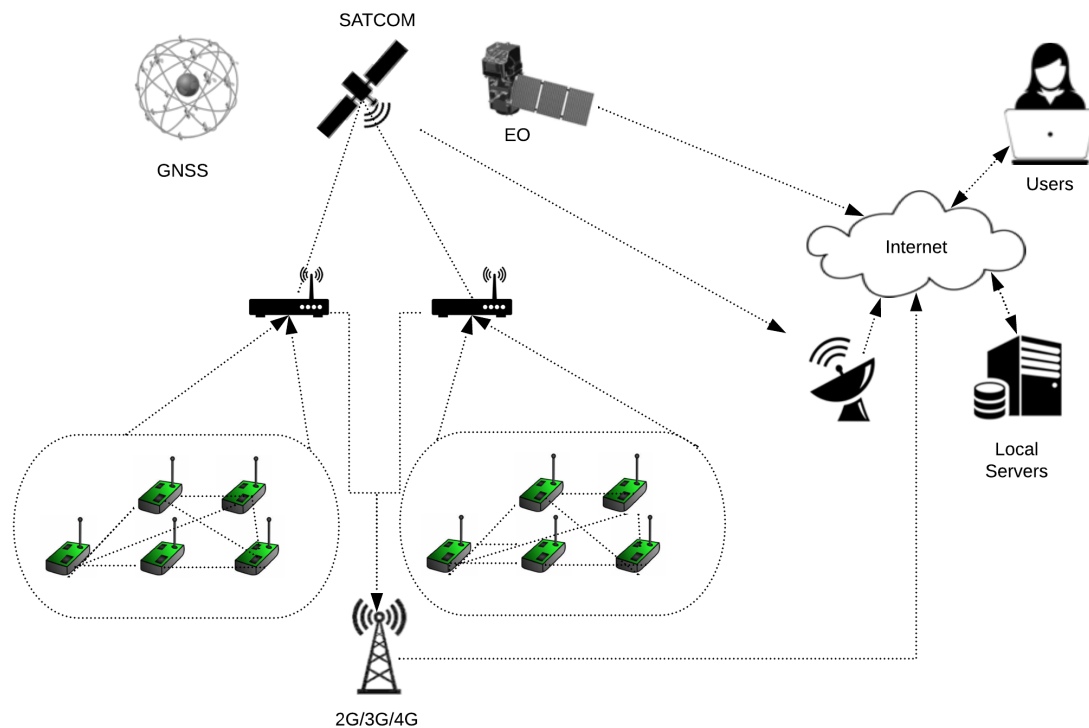


Figure 1. Overview of system architecture.

2.2. Controller Board

The PentaSense board connects up to five external sensor or communication devices with the main controller (Figure 2). It also provides the flexibility to be AC or DC powered and can be configured using a USB-HDI connection. The board has an integrated RF-communication module which operates on the 866 MHz frequency. Optimized time-division multiplexing based meshed routing protocol is implemented on the board to overcome communication distance limitations. The controller board is built around a PIC18F46J50 microcontroller which supports a range of features that can significantly reduce power consumption during operation such as alternate run modes, multiple idle modes, and on-the-fly mode switching.

This can be done by using several techniques such as clocking the controller from the timer source or the internal RC oscillator (up to 90% reduction), the control can remain operational with only the peripherals active on the CPU core disabled.

A fully-featured USB communications module with a built-in transceiver that is compliant with the USB Specification Revision 2.0 is incorporated with low-speed and full-speed communication. The controller board provides ample room for application code, from 16 Kbytes to 64 Kbytes of code space.

The Flash cells for program memory can sustain up to 10,000 erase/write cycles, while data retention is over 20 years. It is possible to read/write the flash program memory during normal operation. The PIC18F46J50 family also provides plenty of room for dynamic application data with up to 3.8 Kbytes of data RAM. The board incorporates a range of serial and parallel communication peripherals. This device also includes two independent Enhanced USARTs and two Master Synchronous Serial Port (MSSP) modules, capable of both Serial Peripheral Interface (SPI) and I2C™ (Master and Slave) modes of operation. The board provides five antilog A/D converters with a

sampling frequency up to 100 KS/s. The 5 A/D conversion channels are time multiplexed. The board can operate between 2.15 V–3.6 V.

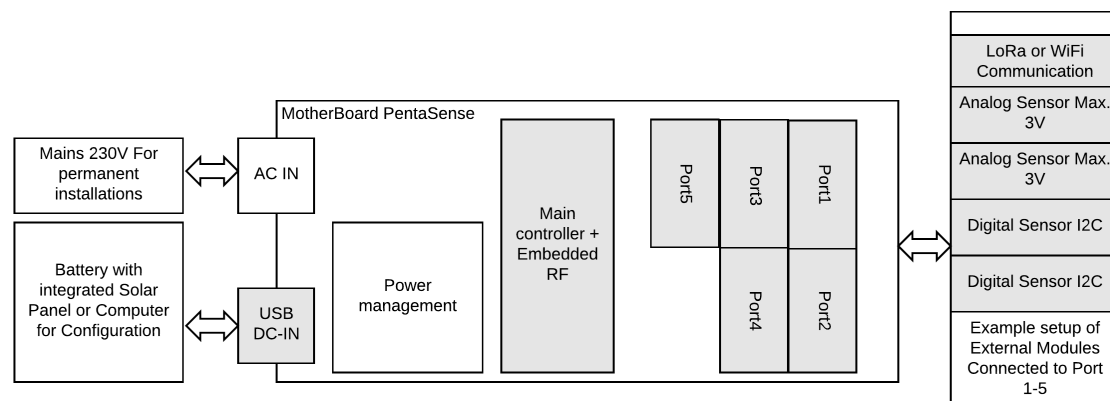


Figure 2. Basic architecture of the PentaSense WSN node.

2.3. Communication Module

2.3.1. RF Communication Module

The communication board contains a fully integrated ISM Band Sub-GHz Transceiver (MRF89XA). The MRF89XA is a single chip, multi-channel FSK/OOK transceiver capable of operating in the 863–870 MHz license-free ISM frequency bands. The MRF89XA module is optimized for very low power consumption and supports data rates up to 200 kbps. It incorporates a baseband modem with data handling features that include a 64-byte FIFO, packet handling, automatic CRC generation, and data whitening. The size and compact architecture allows for flexible integration.

The RF (radio frequency) communication parameters are made programmable and most of them may be dynamically set. The MRF89XA uses several low-power mechanisms to reduce overall current consumption and extend battery life. The MRF89XA complies with European (ETSI EN 300-220) and United States (FCC Part 15.247 and 15.249) regulatory standards.

The RF communication module is equipped with a wide-band half-duplex transceiver, and it supports proprietary sub-GHz wireless protocols and power-saving modes. The operating voltage is 2.1–3.6 V with low current consumption typically -3 mA in receiver mode; -25 mA at $+10$ dBm in transmitter mode, and $1-2$ μ A in Sleep mode. It is operational in temperature ranges from -40 °C to 85 °C which make it well suited for IPM deployment in harsh environments. Furthermore, the communication module supports high data rates of up to 200 kbps and NRZ coding. It has a wide receiver signal strength with dynamics range (70 dB from RX noise floor). The module houses a built-in synchronizer for incoming data, and clock synchronization and recovery and 64-byte transmit/receive FIFO with preload in standby mode

2.3.2. Satellite Communication

The Rockblock Mk2 module for satellite communication [34] was chosen to test the integration abilities of satellite communication in the PentaSense smart gateway. Both evaluation modules are based on the Iridium 9603(N) Short Burst Data Module which can be configured through a serial interface by means of AT-commands, UART interface. The RockBlock 9603 module has a serial interface over USB which allows for configuration and communication with the module. The module supports a two-way communication with global coverage. The power supply needs to be of minimum 100 mA at 5 V DC, however, it can also run the unit directly from a 3.7 V DC LiPo/Lilon battery.

2.3.3. LoRa Communicaiton Module

The LoRa module can be interconnected with the communication ports (Port 1-5; Figure 2) of the PentaSense wireless sensor node. The LoRa module is based on Microchip's RN2483 Low-Power Long Range LoRa Technology Transceiver module provides an easy to use, low-power solution for long-range wireless data transmission. The RN2483 radio complies with the LoRaWAN Class A protocol specifications. It integrates RF, a baseband controller, command Application Programming Interface (API) processor, making it a complete long-range solution.

The communication module houses an onboard LoRaWAN protocol stack which with ASCII command interface over a universal asynchronous receiver-transmitter (UART) and possible device firmware upgrade (DFU) over it. The compact size of the module makes it easy to attach and house within the same environmental shelter as the smart gateway with castellated SMT pads for PCB mounting. This module is operational in the same range as the RF communication module making it easy to combine, it has lower power consumption with programmable RF communication bit rate up to 300 kbps with frequency shift keying modulation. The model has an integrated microcontroller unit, radio transceiver with an analog front end and 14 general-purpose input/outputs for control and status. The module is equipped with the RF analog feature able to operate on 866 MHz frequency bands hence eliminating the need for integrating both modules for low-range point to point within the mesh as well as long-range gateway-to-gateway communication. The TX power is adjustable up to +14 dBm with high-efficiency power amplifiers. The range can go up to 15 km at a suburban and 5 km in an urban area of course depending on the elevation profile.

2.4. Embedded Energy Harvesting

The PentaSense module has the ability to be powered through the USB connector. This gives the flexibility to use any of the shelf waterproof power banks with an integrated solar cell for autonomous use. Depending on the number of attached sensors and the expected data rate, a power bank with a minimum capacity of 5000 mAh is used. Current power banks deliver much higher capacities and provide as such much more reliable autonomy for the sensor nodes. A rule of thumb for the capacity estimation is:

$$PowerBankCapacity = [(DCRF \cdot 15) + (DCL \cdot 30) + \sum (DCS_i \cdot PS_i)] \cdot 24 \cdot D_{aut} \quad (1)$$

where DCR is the duty cycle time of low power radio in daily percentage, DCL is the duty cycle time of LoRa in daily percentage, DCS_i is the duty cycle time of $Sensor_i$ in daily percentage, PS_i is the power used by $Sensor_i$, and D_{aut} stands for the days of guaranteed autonomy (Battery requires 18 h of direct sun complete charging)

The SIMICO S3 Foldable Solar powerbank (10.000 mAh) was chosen among a set of 6 candidates, mainly because it can support experiments with different sizes of the solar panel area. It has a capacity of 10.000 mAh, internal batteries, four solar panels and 2 USB connections (2×1000 mA, 5V).

2.5. Gateway

A dual-core tablet running on Windows 10 was used as a gateway prototype for the PentaSense system (Figure 3). It takes the role of managing the data-storage, to make the decisions regarding the choice for the communication medium and interfaces to external communication and localization peripherals. The tablet acts as the central sink for the WSN, and is a communication hub for the SatCom short messages, to communicate through 3 G or GPRS, and to create a precise anchor localization through GPS.

This architecture allows us to rapidly prototype and test the envisioned gateway functionalities. It can also be very useful due to the availability of a display which can be used as a keyboard-less interface for on-field configuration of the system. Moreover, it also allows for tethering with a smartphone in case the tablet is sealed in an environmental shield or just placed and remote

configuration by a smartphone is necessary. The tablet also incorporates a low power SSD hard disk to achieve long term data-retention and operate in a low power-consumption mode. Data compression and data aggregation is applied before sending the data through payed connections.

With an external solar panel and battery, the system can operate autonomously for several weeks or even months. This requires further optimization of the OS. To increase the autonomy of the gateway, it is necessary for the tablet to go regularly in sleep mode or at least to turn off the display when no user interaction is required. Putting the tablet in sleep mode might lead to specific problems regarding the power provision of the communication peripherals. To avoid this, it is necessary to enable USB power availability when in sleep mode and to set-up wake up timers.

To monitor the system and to provide a way to remotely upgrade the gateway, we have investigated off the shelf tools for remote access support. In this study, we examined two tools—a freeware tool (The Cloudberry Remote Assistant [35]) and a licensed tool (Teamviewer [36]). This remote access tool allows for taking over all the functionalities of the Windows-based smart gateway. It can restart the gateway and send over files to perform a local upgrade of the gateway. The greatest advantage of this tool is that it can be set up for unattended access. All users with the access key can remotely access the system and no personal interaction is required. A disadvantage of the tool is that a Windows system is required to perform the remote access. It does not support tablets or smartphones. The TeamViewer software is a commercial tool which is used worldwide and provides the ability to incorporate the functionalities in your own application. This means that it is not necessary to install a separate remote access software once compiled into your own application. It is a proven tool and is used by many companies for remote assistance. The tool is very well designed and gives remote access to the smart gateway trough many devices. We have positively tested remote access through an Android smartphone. Other devices like tablets are also supported. One disadvantage of the tool is that it does not support unattended access by default. This means that once the smart gateway reboots, a local person should send over the auto-generated access-key (password) to re-establish a connection. During the tests, it happened that we lost control over the machine and a person had to be sent to retrieve the key from the smart gateway. The software, however, can provide permanent access to a remote computer (i.e., our smart gateway) through a mechanism of partner-list. This tool is not free and requires a yearly fee per user.

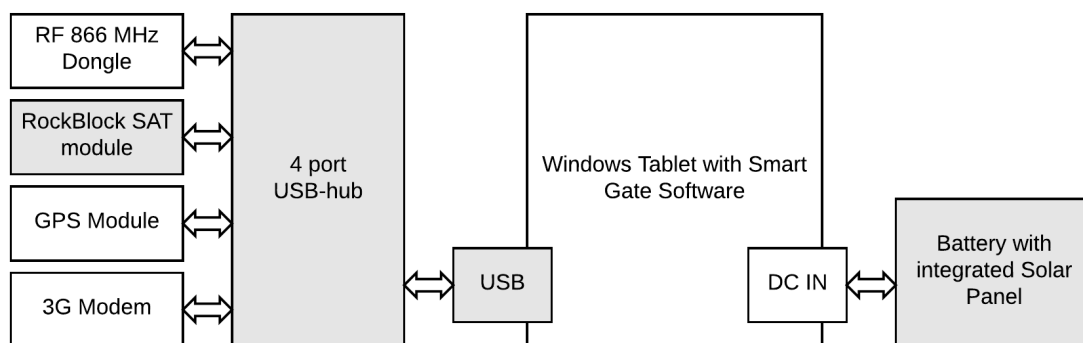


Figure 3. Basic architecture of the PentaSense WSN gateway.

2.6. SDSS

The WSN and EO data are stored in a database and fed to the SDSS which is run on a remote server. Due to the high modularity of the WSN system the SDSS can support numerical models that generate the following outputs for different pest species and diseases: (i) Hotspot analysis and risk maps; (ii) Population Dynamics Forecasts and Alarms; (iii) Disease risk assessment. It is envisioned as an administrative tool for IPM applications. The backend to the SDSS uses the following technologies: C# with ILNumerics library for in-house developed algorithms. ILNumerics can be used under a

commercial license. The SDSS uses SailsJS together with the Angular framework. SailsJS acts as the backend, hosting all the API endpoints and handling the database requests. Angular acts as frontend, loading all needed data from the API and visualizing this data in a web browser. Moreover, the Iridium RockBlock module at the WSN sink, provides basic communication services which can be easily activated and followed up using a generic web application.

It can integrate products such as MODIS and Sentinel. MODIS is widely used in the field of spatial modeling and offers several very useful products. Standard derivatives as normalized difference vegetation index (NDVI) and enhanced vegetation index (EVI) are widely accepted standards in environmental modeling. Other derivatives such as day and night surface temperature are useful in specific models. This data is supplemented with multi-year averages such as WorldClim version 2 data [37]. The MODIS (moderate-resolution imaging spectroradiometer) instrument is built by Santa Barbara Remote Sensing and is installed on two satellites: Aqua and Terra. The Modis instrument captures 36 spectral bands in 0.4–14.4 μm wavelength range. Its spatial resolution varies depending on the band: 250 m for bands 1–2, 500 m for bands 3–7 and 1000 m for bands 8–36.

The Sentinel missions are part of the Copernicus program, which is the European earth observation mission coordinated by the European Commission together with ESA. With the recent launch of the Sentinel-2b satellite, Copernicus has now a temporal resolution of 5 days. Sentinel 2 has three different spatial resolutions (10, 20 and 60 m) and 13 spectral bands in the visible and near infrared (VNIR) and short-wave infra-red (SWIR).

On Figure 4 the conceptual layout of the SDSS is shown. Parameters such as specific user parameters (number of field sites, pest data etc.), the spatial scale, and type of model are set at the start of the integration. On the other hand the control action parameter acts as a dynamic external forcing parameter that can be supplied to the already running numerical integration.

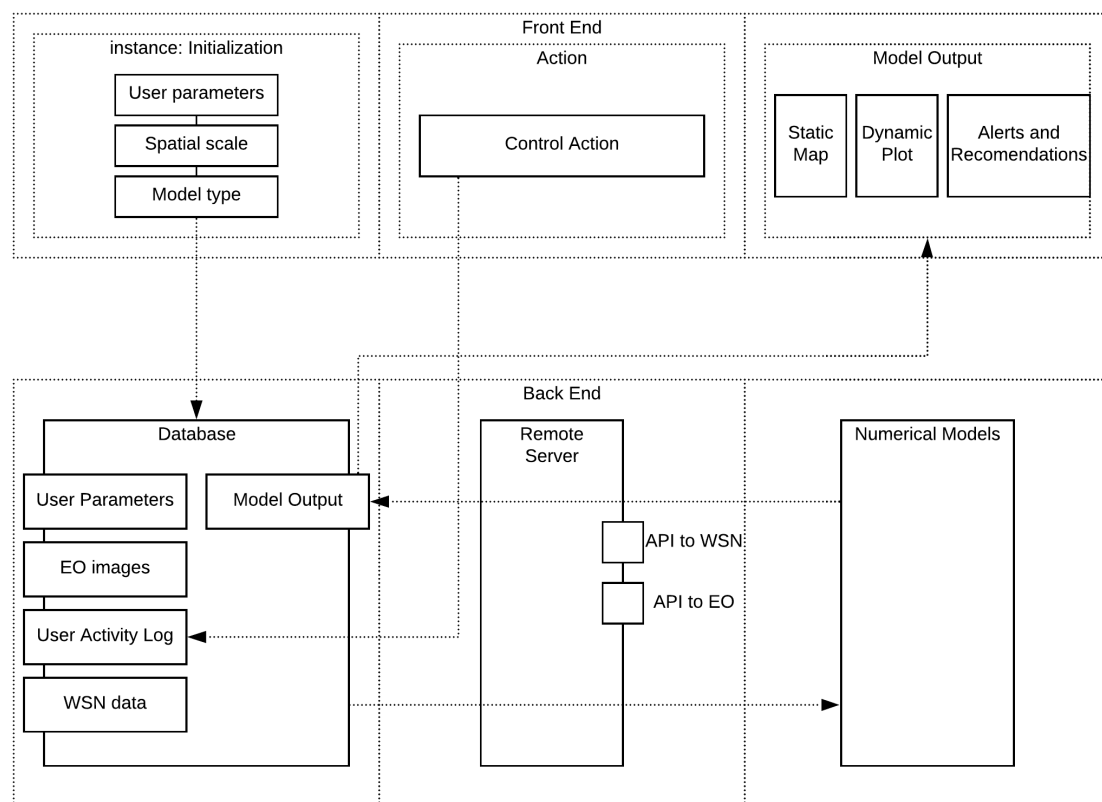


Figure 4. Conceptual layout of the spatial decision support system.

The total cost of the hardware is estimated at €1874 for a system consisting of: One gateway with a satellite communication module, terrestrial communication module and energy harvesting device;

and six PentaSense boards measuring temperature, relative humidity and pressure with an external energy harvesting solution. Additionally, the cost of maintaining the SDSS is estimated at € 180 per user annually, making the total cost of implementation € 2024.

Case Study: ASSESSING the Climatic Suitability for the Establishment of *Aedes albopictus* in Belgium

Two possible outputs of the SDSS models were explored. A statistical analysis of general climatic suitability and single-point dynamical simulations for an invasive mosquito species *Ae. albopictus* for Belgium and a population dynamics model forced by the WSN data. The data was processed in the R-project software environment ([38]).

(a) MCDA model simulating the climatic suitability of *Aedes albopictus* in Belgium:

To look at the climatic suitability for the establishment of the invasive mosquito species *Ae. albopictus* in Belgium we employed a mechanistic Multi-Criteria Decision Analysis model following previous work of Petrić et al. [39,40]. This model consists of sigma fuzzy membership functions used to map the suitability corresponding to climatic thresholds limiting the ability of the vector to overwinter and reproduce during the active season.

The climatic parameters (30-year averages for the reference period 1971–2000) that were selected as input to the model are: (i) Mean annual temperature; (ii) Total annual precipitation; (iii) Mean temperature for June, July, and August; (iv) Mean January temperature and (v) Precipitation frequency expressed as number of days within a year with rain >1 mm. Finally, we use NTL (night-time light) [41] remote sensed data as a proxy for human population density and outputs from a digital elevation model for estimating the vertical temperature gradient during the interpolation with the co-Kriging algorithm.

The climate data were obtained from the WorldClim online database [37] with a resolution of 30 arc-seconds (≈ 1 km).

(b) WSN as input to a dynamical *Ae. albopictus* population model:

For this paper, we looked at the output from a pilot test of the PentaSense system in a field site in Sint Truiden (Belgium) at the Pcfuit institute [42]. The nodes cover an area of approximately 1.4 ha. Temperature data has been collected from September 2018 and is still in place. The system consists of 4 PentaSense nodes using Lora and RF 866 MHz point to point communication and a smart Gateway with the RockBLoK 9603 SBD Module and 3G communication Modem. The SDSS generates forcing time-series files based on input from the Wireless Sensor Network.

The dynamic model consists of a nonlinear, coupled set of 10 prognostic ordinary differential equations focusing on the main phases in the life cycle of the pest [43]. The model is integrated with a daily time step using an implicit Adams numerical scheme and forced with temperature-dependent external parameters.

Finally, we compare the WSN data that was used to force the mosquito population dynamics model with long term averages for the current climatology (reference period 1981–2010). For this, we used the ERA5 re-analysis data from ECMWF [44] which offers hourly time series of surface variables on a 30 km grid. The grid point nearest to the WSN was selected.

3. Results

3.1. Testing the WSN

Several tests were performed to get the primary metrics describing the Quality of Service (QoS) provided by the PentaSense WSN. These measurements give us statistical data that can support different configurations of the network. Moreover, the results highlight the factors that need to be considered when testing WSN networks within the IPM framework. A summary of the results is shown in Table 1.

Table 1. Summary of test results.

| Test Name | Test Parameters | Measured | Target |
|------------------------------|---|----------------------------|-------------------|
| Signal Strength | RockBlock signal strength; cloud cover 10/10; raining | 1 | ≥ 3 |
| | RockBlock signal strength; cloud cover 10/10; no rain | 2 | ≥ 3 |
| | RockBlock signal strength; cloud cover 5/10; no rain | 3 | ≥ 3 |
| | RockBlock signal strength; cloud cover 3/10; no rain | 4 | ≥ 3 |
| | RockBlock signal strength; cloud cover 0/10; no rain | 5 | ≥ 3 |
| Data Loss | Number of transmissions | 100 | 100 |
| | Number of packets billed | 100 | 100 |
| | Number of packets received | 96 | 90 |
| Bandwidth | No of packets with full pay-load (340 bytes)/min | 20 | >6 |
| Coarse Grain Localization | Localization error; RockBlock signal strength 5 | <2 km | - |
| | Localization error; RockBlock signal strength 4 | <5 km | - |
| | Localization error; RockBlock signal strength 3 | <15 km | - |
| | Localization error; RockBlock signal strength 2 | <30 km | - |
| | Localization error; RockBlock signal strength 1 | >30 km | - |
| Point to point communication | Maximum data rate; 50 m distance | 48 kbps | Max data loss <2% |
| | Maximum data rate; 40 m distance | 64 kbps | Max data loss <2% |
| | Maximum data rate; 30 m distance | 128 kbps | Max data loss <2% |
| | Maximum data rate; 20 m distance | 256 kbps | Max data loss <2% |
| Energy autonomy | Still alive signal at 0 dBm to sink every 10 s | 75% charged at end of test | Min 8 weeks |
| Mesh network configuration | 15 sensor, 30 m, 48 kbps | 15 | 15 |
| Automated discovery | Automatic discovery of 15 sensors by the gateway | <30 s | <1 min |
| Data loss test | 24 h; number of allowed retransmissions 0 | <3% | <1% |
| | 24 h; number of allowed retransmissions 1 | <1% | <1% |
| | 24 h; number of allowed retransmissions 2 | <0.2% | <1% |
| | 24 h; number of allowed retransmissions 3 | <0.2% | <1% |
| | 24 h; number of allowed retransmissions 4 | <0.2% | <1% |

3.1.1. Testing the SatCom Module

Software in C# was developed to test the SatCom module so that it could be easily configured. The developed software allowed us to test the following parameters of the RockBlock SBD module: (a) Signal quality with use of embedded antenna; (b) Data loss and reliability; (c) Bandwidth; (d) Use of course grain localization by means of trilateration without use of GNSS.

- (a) *Signal strength*: The signal strength is examined on a 0–5 level scale, 0 meaning no connection and 5 signifying maximum signal strength. Signal strength was 0 for cases where the module did not have a clear view of the sky. When placed outdoors, the test demonstrated signal attenuation as a function of cloud cover and precipitation. Signal strength varied between 1 and 5. A reliable connection (≥ 3) was reached when cloud cover was less than 5/10. Concerning precipitation, the extent of signal attenuation depends on the rate as well as on the raindrop size. The interference during the test was significant, reducing the signal to 0.
- (b) *Data Loss*: Since the RockBlock SBD module does not store information for tracking the number of lost data packages, for the purpose of this test we developed a set with sequenced, numbered and time-stamped data packets with the maximum payload (i.e., 340 bytes). The test was carried out on three segments of the communication chain: (i) The number of transmissions requested by the sink; (ii) number of transmissions billed by the RockBlock data-operator; and (iii) number of packets received at the sink. Two configuration bugs were discovered: a discrepancy in the number of sent and number of billed packets which can be attributed to the module itself, and another between the number of billed and the number of packets received at the sink which is related to the signal strength. Namely, when the signal strength is below 3 some packets that were billed were not received at the sink.
- (c) *Bandwidth*: The RockBlock 9603 SBD module operates with RF between 1616–1626.5 MHz. The bandwidth depends heavily on weather conditions such as cloud cover, precipitation and in a lesser manner temperature and relative humidity. The attenuation effect of rain depends on the ratio of the corresponding uplink wavelength and raindrop diameter. We were able to send up to 20 data-packets with full payload per minute without data loss under ideal signal conditions (level 5).
- (d) *Course Grain Localization*: The communication module provides very basic course grain localization without the need for an extra GPS module, reducing the overall cost of the system. The localization precision exhibited significant variation with the radius between 2 and 30 km depending on the strength of the SatCom signal.

3.1.2. Testing the WSN Nodes

- (a) *Point to point communication*: Firstly, the maximum distance between the sensor and sink was determined as the distance at which RSSI is 0 dBm (1 mW). Indoors this value was 50 m. Secondly, we consider data rates at different increments of the maximum distance (50 m), while keeping the data loss rates below 2%. The rate was 48 kbps up to approximately 50 m (maximum distance), 64 kbps up to approximately 40 m, 128 kbps up to approximately 30 m 256 kbps (maximum data rate) up to approximately 20 m.
- (b) *Energetic autonomy*: The test performed consists of communicating a ‘still alive signal’ at 0 dBm to the sink every 10 s. Full Energetic autonomy was achieved during the test (8 weeks) based on a 10,000 mAh solar chargeable power bank. The power bank was still 75% charged at the end of the test. The solar panels of the power bank were positioned behind a window in North-East direction.
- (c) *Mesh network configuration*: An extended indoor lab test which consists of 15 sensors has been performed. The sensors have been distributed in a three-story building, with 5 sensors on each floor. The size of the building is approximately 30 m by 120 m. Each floor has a height of 4 m.

The distance between the sensors was typically 30 m, the data rate was set to 48 kbps. The test was performed successfully with this configuration.

- (d) *Automated discovery*: This test was performed to evaluate the speed and ability of the sink to discover new nodes as they are introduced. For a set of 15 newly introduced sensors, the discovery time was below 30 s.
- (e) *Data loss*: In this test, we take a look at the number of lost data-packets due to interference, packet collisions or other unknown influences. We found that the results depend chiefly on the number of allowed transmissions (Table 1). The system was observed for 24 h with the sensing duty cycle set to 1 sample per minute with packet size of 24 bytes. The proprietary routing protocol was based on time-division multiplexing over the network mesh.

3.2. Case Study: *Aedes albopictus* in Belgium

On Figure 5. The static map for the suitability of establishment of *Ae. albopictus* in Belgium is shown. This static map is based on climate normals (i.e., 30-year averages) of the climate variables. After the initial computation, it is stored in the SDSS database and called as input for defining the eco-climatic zones with reference to which the dynamical model is called. We see that Belgium is suitable for the establishment of *Ae. albopictus* with a clear difference between the densely populated north and the south which has a smaller density of population and higher altitudes that affect the overwintering suitability for the mosquito vector.

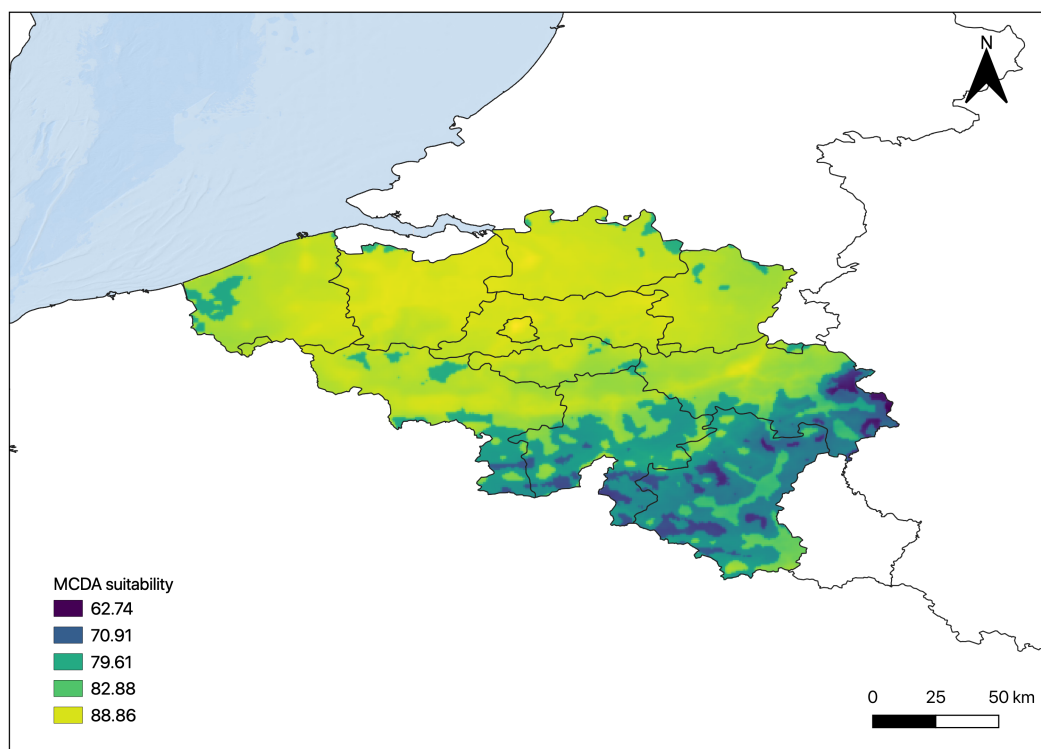


Figure 5. Climatic suitability for the establishment of *Ae. albopictus* in Belgium based on outputs from the MCDA model.

The output from the population dynamics simulations for *Ae. albopictus* forced by the WSN measurement for one month (18 September–18 October 2019) is shown in Figure 6. This model is forced with a daily time-step; the input from the WSN is aggregated at the end of each day and appended to the model forcing file.

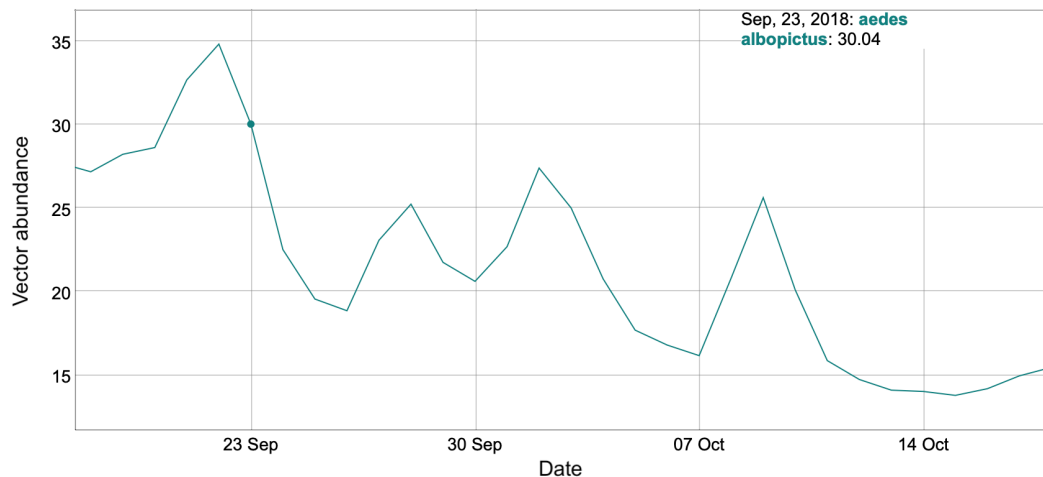


Figure 6. Simulated population dynamics for *Ae. albopictus* based on the measured temperature from the PentaSense WSN for the period 18 September 2018–18 October 2018.

The dynamics exhibits a negative trend which corresponds to the expected reality for the vector. The population experiences a drop until a specific temperature and photoperiod threshold is met and the adults die-off. Only the eggs transition into the next year.

The WSN provides accurate forcing that is specific to the pest microhabitat. Another important aspect of having site and time specific forcing is emphasized in Figure 7 where we look at the deviation of the measured temperature value from the 30-year ensemble for the same period within the reference period (1981–2010). We see that for this specific model run the temperature was significantly higher than the climatology. This influences the mosquito activity and onset of autumn diapause.

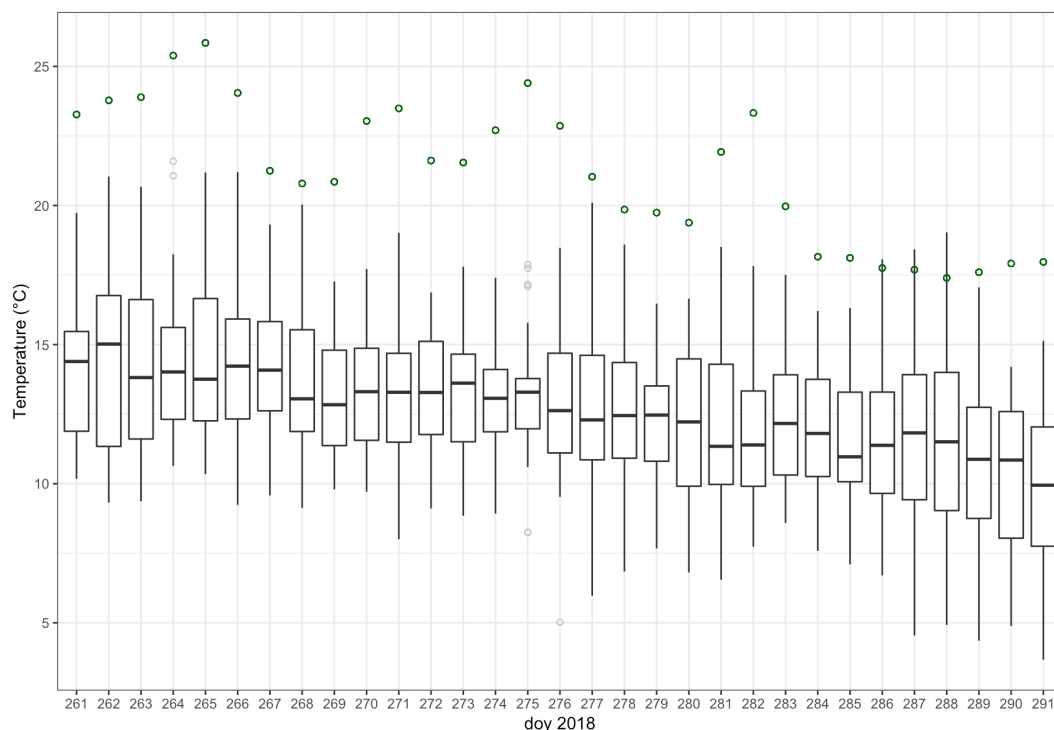


Figure 7. A comparison of the observed WSN temperature values (dark green) and the ERA5 1981–2010 climatology (box plot) for the period indicated 18 September (261 day) to 18 October (291 day).

4. Discussion

In this paper, we described our experimental PentaSense WSN network set-up in a field site in Belgium and output generated by two models related to the climatic suitability for the establishment and meteorological suitability driving the inter-annual dynamics of the mosquito vector *Ae. albopictus*. Thus, we examined the feasibility of integrating an autonomous low-cost wireless sensor network with a spatial decision support system meeting the specific requirement of IPM applications.

We designed, executed and analyzed a set of tests evaluating the basic Quality of Service of the WSN. Firstly, the following metrics were considered for the SatCom module: (i) Signal Strength; (ii) Data Loss; (iii) Bandwidth; and (iv) Course Grain Localization. Secondly, for the WSN nodes we performed tests for the following functionalities: (i) Point-to-point communication; (ii) Energy autonomy; (iii) Mesh network configuration; (iv) Automated node discovery; and (v) Data loss. The results showed that the signal strength of the SatCom module was highly dependent on the fraction of the sky obscured by clouds, and for values above 5/10, the signal strength would be low enough to cause data loss which was observed in the number of billed and received data packets. During the test, we discovered several configuration bugs which lead to loss of data due to the SatCom module itself. Our best guess is that this happens when a data packet is received at the server of the service provider, but the CRC shows a malicious receipt. The packet is billed, but not sent to the end-application due to data corruption. This only happens under the condition that the signal strength is below level 3. This type of data loss can be avoided by having the data sent only when the signal strength is 3 or higher. The system performed well regarding the evaluated metrics and met the criteria for IPM deployment.

The WSN is suitable for large-scale as well as small-scale applications. The scale of the system will significantly depend on the pest species and type of real-world deployment. For certain mosquito vectors small-scale monitoring with a denser sensor network is important to capture the micro-climatic conditions of the resting habitats; while, for example, for the olive fruit fly (*Bactrocera oleae*) sensors coupled with automated traps are used on larger spatial scales with a less dense network to monitor the population across the orchards which can span from 100–500 trees for small orchards in Turkey to 2000–5000 trees for big orchards which are typical for Spain and Australia. The system has a high degree of modularity in terms of the spatial scale of deployment due to the global coverage of the Iridium SBD module as well as high availability of public LoRa providers, with LoRaWAN being the leading open global standard for secure LPWAN connectivity and wide range communication. For small inter-node distances of up to 50 m, the nodes communicate with RF while for greater distances the system uses LoRa communication, while the traffic load and number of nodes in our application was small. The total network yield for standard IPM applications (up to 30 nodes per ha) is still relatively low and will not impact data loss due to delivery or end-to-end delay.

The outputs of the suitability model for *Ae. albopictus* are in accordance with previously published work [45–47] indicating that Belgium is suitable for the establishment of the invasive vector species. *Ae. albopictus* has last been detected in 2016 [48] and previously in 2013 and 2014 [49]. The mosquito is still not established in Belgium, however, is crossing the border from neighboring countries such as Germany and France. The spread needs to be closely monitored to prevent the mosquito from gaining a foothold in Belgium. Models supported by WSN data can guide surveillance and monitoring efforts on a country level.

Although we cannot test the simulated population dynamics it exhibits a realistic trend in which the population density decreases up to the diapausing threshold defined by critical values for temperature and photoperiod [50]. Higher temperatures indicated in Figure 7 lead to a shift of diapause date to a later time thus prolonging the seasonal activity of the disease vector.

Climate change projections indicate that by the end of the century Belgium is expected to undergo a significant rise in temperature, 1.7–4.9 °C for winter and 2.4–6.6 °C for summer. However, climate change will also lead to a possible increase in extreme events such as heat stress and cooling degree

days as well as extreme values for maximum and minimum temperatures [51,52] making it essential to register extreme events on a local scale with high temporal resolution to inform timely action.

The PentaSense network is currently being tested in field settings and the next step will be testing the software for the dual-uplink as well as the robustness of system hardware in remote areas and harsh environmental conditions. Considerations need to be taken so that the WSN is deployed in ways that capture land use heterogeneity. Suitable biotopes for sensor placement and sensor density can be identified using EO. Moreover, on-site tests should always be conducted to test validity and reliability.

WSN in combination with cloud services and satellite technologies have the potential to have great impact on the way IPM is conducted worldwide. New algorithms that allow for the combination of ground measured and modeled data at multiple scales will provide information on when and how to conduct pest control with minimal impact on the environment.

Author Contributions: Conceptualization, M.P., E.D. and A.T.; Data curation, M.P. and A.T.; Formal analysis, M.P., J.V. and A.T.; Funding acquisition, M.P., C.M., E.D. and A.T.; Investigation, M.P., J.V., C.M. and A.T.; Methodology, M.P., C.M., E.D. and A.T.; Project administration, M.P., E.D. and A.T.; Resources, M.P., E.D. and A.T.; Software, M.P., J.V., T.M. and A.T.; Supervision, E.D. and A.T.; Validation, M.P. and A.T.; Visualization, M.P.; Writing—original draft, M.P., C.M. and A.T.; Writing—review & editing, M.P., J.V., C.M., T.M., E.D. and A.T.

Funding: The work described in this paper was realized as a part of the feasibility study ‘SenZitall’ co-funded by ESA, under the Integrated Applications Program.

Conflicts of Interest: The authors declare no conflict of interest.

Abbreviations

The following abbreviations are used in this manuscript:

| | |
|-------|---|
| API | Application Programming Interface |
| CRC | Cycle Redundancy Check |
| EO | Earth Observations |
| IPM | Integrated Pest Management |
| MCDA | Multi Criteria Decision Analysis |
| NRT | Near Real Time |
| NRZ | Non Return To Zero |
| PCB | Printed Circuit Board |
| RF | Radio Frequency |
| SBD | Short Burst Data |
| SMT | Surface Mount Technology |
| SPI | Serial Peripheral Interface |
| USART | Universal Synchronous/Asynchronous Receiver/Transmitter |
| WAN | Wide Area Network |
| WSN | Wireless Sensor Network |

References

1. World Health Organisation. Vector Borne Disease. Available online: <https://www.who.int/news-room/fact-sheets/detail/vector-borne-diseases> (accessed on 14 April 2019).
2. Gartner. Newsroom: Press Release. Available online: <https://www.gartner.com/technology/pressRoom.do?id=3598917> (accessed on 14 April 2019).
3. Das, S.; Maitra, A.; Shukla, A.K. Rain attenuation modeling in the 10–100 GHz frequency using drop size distributions for different climatic zones in tropical India. *Prog. Electromagn. Res.* **2010**, *25*, 211–224. [CrossRef]
4. Sharma, A.; Jain, P. Effects of rain on radio propagation in GSM. *Int. J. Adv. Eng. Appl.* **2010**, *2010*, 83–86.
5. MODIS. NASA, Moderate Resolution Imaging Spectroradiometer. Available online: <https://modis.gsfc.nasa.gov/data/> (accessed on 14 April 2019).
6. Sentinel Mission. ESA, Sentinel-2 Data Products. Available online: <https://sentinel.esa.int/web/sentinel/missions/sentinel-2/data-products> (accessed on 14 April 2019).

7. Rochlin, I.; Ninivaggi, D.V.; Hutchinson, M.L.; Farajollahi, A. Climate change and range expansion of the Asian tiger mosquito (*Aedes albopictus*) in Northeastern USA: Implications for public health practitioners. *PLoS ONE* **2013**, *8*, e60874. [[CrossRef](#)] [[PubMed](#)]
8. De Roeck, E.; Van Coillie, F.; De Wulf, R.; Soenen, K.; Charlier, J.; Vercruyse, J.; Hantson, W.; Ducheyne, E.; Hendrickx, G. Fine-scale mapping of vector habitats using very high resolution satellite imagery: A liver fluke case-study. *Geospat. Health* **2014**, *8*, S671–S683. [[CrossRef](#)] [[PubMed](#)]
9. Mairota, P.; Cafarelli, B.; Labadessa, R.; Lovergine, F.; Tarantino, C.; Lucas, R.M.; Nagendra, H.; Didham, R.K. Very high resolution Earth observation features for monitoring plant and animal community structure across multiple spatial scales in protected areas. *Int. J. Appl. Earth Obs. Geoinf.* **2015**, *37*, 100–105. [[CrossRef](#)]
10. Datir, S.; Wagh, S. Monitoring and detection of agriculture disease using WSN. *IJCA* **2014**, *87*, 09758887. [[CrossRef](#)]
11. Srivastav, N.; Chopra, G.; Jain, P.; Khatter, B. Pest Monitor and control system using WSN with special reference to Acoustic Device. *J. Entomol. Zool. Stud.* **2013**, *3*, 92–99.
12. Srinivas, S.; Harsha, K.; Sujatha, A.; Kumar, N.G. Efficient Protection of Palms from RPW Larvae using Wireless Sensor Networks. *Int. J. Comput. Sci. Issues* **2013**, *10*, 192–200.
13. Al-Manie, M.A.; Alkanhal, M.I. Acoustic detection of the red date palm weevil. *Int. J. Signal Process.* **2004**, *1*, 1–12.
14. Azfar, S.; Nadeem, A.; Basit, A. Pest detection and control techniques using wireless sensor network: A review. *J. Entomol. Zool. Stud.* **2015**, *3*, 92–99.
15. Bajwa, W.I.; Coop, L.; Kogan, M. integrated pest management (IPM) and Internet-based information delivery systems. *Neotropical Entomol.* **2003**, *32*, 373–383. [[CrossRef](#)]
16. University of California, Agriculture and Natural Resources. DD Models: Insects, Mites, Diseases, Plants, and Beneficials. Available online: <http://ipm.ucanr.edu/MODELS/index.html> (accessed on 20 May 2019).
17. Uspect—Agricultural, Pest Management, and Plant Biosecurity Decision Support in the US. IPM Pest and Plant Disease Models and Forecasting. Available online: <http://pnwpest.org/wea> (accessed on 20 May 2019).
18. Southwest Technical Resource Center for School IPM. IPM Cost Calculator. Available online: <http://www.ipmcalculator.com/> (accessed on 20 May 2019).
19. University of California, Agriculture and Natural Resources. California PestCast: Disease Model Database. Available online: <http://ipm.ucanr.edu/DISEASE/DATABASE/diseasemodeldatabase.html> (accessed on 20 May 2019).
20. Damos, P. Modular structure of web-based decision support systems for integrated pest management. A review. *Agron. Sustain. Dev.* **2015**, *35*, 1347–1372. [[CrossRef](#)]
21. Brown, J.H. On the relationship between abundance and distribution of species. *Am. Nat.* **1984**, *124*, 255–279. [[CrossRef](#)]
22. Rousse, P.; Gourdon, F.; Roubaud, M.; Chiroleu, F.; Quilici, S. Biotic and abiotic factors affecting the flight activity of *Fopius arisanus*, an egg-pupal parasitoid of fruit fly pests. *Environ. Entomol.* **2009**, *38*, 896–903. [[CrossRef](#)] [[PubMed](#)]
23. Patz, J.; Githeko, A.; McCarty, J.; Hussein, S.; Confalonieri, U.; De Wet, N. Climate change and infectious diseases. *Clim. Chang. Hum. Health Risks Responses* **2003**, *2*, 103–132.
24. Poveda, G.; Graham, N.E.; Epstein, P.R.; Rojas, W.; Quiñones, M.L.; Velez, I.D.; Martens, W.J. Climate and ENSO variability associated with vector-borne diseases in Colombia. *El Niño South. Oscill. Multiscale Var. Glob. Reg. Impacts* **2000**, *1*, 183–204.
25. Harvell, C.; Kim, K.; Burkholder, J.; Colwell, R.; Epstein, P.R.; Grimes, D.; Hofmann, E.; Lipp, E.; Osterhaus, A.; Overstreet, R.M.; et al. Emerging marine diseases—climate links and anthropogenic factors. *Science* **1999**, *285*, 1505–1510. [[CrossRef](#)]
26. Hales, S.; Weinstein, P.; Soares, Y.; Woodward, A. El Niño and the dynamics of vectorborne disease transmission. *Environ. Health Perspect.* **1999**, *107*, 99–102.
27. Abiodun, G.J.; Maharaj, R.; Witbooi, P.; Okosun, K.O. Modelling the influence of temperature and rainfall on the population dynamics of *Anopheles arabiensis*. *Malar. J.* **2016**, *15*, 364. [[CrossRef](#)]
28. Ahumada, J.A.; Laoointe, D.; Samuel, M.D. Modeling the population dynamics of *Culex quinquefasciatus* (Diptera: Culicidae), along an elevational gradient in Hawaii. *J. Med. Entomol.* **2004**, *41*, 1157–1170. [[CrossRef](#)]

29. Paaijmans, K.P.; Imbahale, S.S.; Thomas, M.B.; Takken, W. Relevant microclimate for determining the development rate of malaria mosquitoes and possible implications of climate change. *Malar. J.* **2010**, *9*, 196. [[CrossRef](#)] [[PubMed](#)]
30. IUCNGISD. Global Invasive Species Database. Available online: <http://www.iucngisd.org/gisd/> (accessed on 14 April 2019).
31. Paupy, C.; Delatte, H.; Bagny, L.; Corbel, V.; Fontenille, D. Aedes albopictus, an arbovirus vector: From the darkness to the light. *Microbes Infect.* **2009**, *11*, 1177–1185. [[CrossRef](#)] [[PubMed](#)]
32. Benedict, M.Q.; Levine, R.S.; Hawley, W.A.; Lounibos, L.P. Spread of the tiger: global risk of invasion by the mosquito Aedes albopictus. *Vector-Borne Zoonotic Dis.* **2007**, *7*, 76–85. [[CrossRef](#)] [[PubMed](#)]
33. Waldo, J.; Chandra, N.L.; Lelieveld, J.; Proestos, Y.; Michael, E.; Christophides, G.; Parham, P.E. The role of environmental variables on Aedes albopictus biology and chikungunya epidemiology. *Pathog. Glob. Health* **2013**, *107*, 224–241. [[CrossRef](#)] [[PubMed](#)]
34. Iridium. RockBLOCK Mk2. Available online: <https://www.iridium.com/products/rock-seven-rockblock-mk2/> (accessed on 14 April 2019).
35. CloudBerry Lab. Free Remote Assistance Software for Windows. Available online: <https://www.cloudberrylab.com/remote-assistant.aspx> (accessed on 14 April 2019).
36. TeamViewer. Remote Support, Remote Access, Service Desk, Online Collaboration and Meetings. Available online: <https://www.teamviewer.com/en/> (accessed on 14 April 2019).
37. WorldClim. Global Climate Data—Free Climate Data for Ecological Modeling and GIS. Available online: <http://www.worldclim.org/node/1> (accessed on 14 April 2019).
38. R Development Core Team. *R: A Language and Environment for Statistical Computing*; R Foundation for Statistical Computing: Vienna, Austria, 2008; ISBN 3-900051-07-0.
39. Petrić, M.; Lalić, B.; Ducheyne, E.; Djurdjević, V.; Petrić, D. Modelling the regional impact of climate change on the suitability of the establishment of the Asian tiger mosquito (Aedes albopictus) in Serbia. *Clim. Chang.* **2017**, *142*, 361–374, doi:10.1007/s10584-017-1946-8. [[CrossRef](#)]
40. Petrić, M.; Lalić, B.; Pajović, I.; Micev, S.; Đurđević, V.; Petrić, D. Expected Changes of Montenegrin Climate, Impact on the Establishment and Spread of the Asian Tiger Mosquito (Aedes albopictus), and Validation of the Model and Model-Based Field Sampling. *Atmosphere* **2018**, *9*, 453, doi:10.3390/atmos9110453. [[CrossRef](#)]
41. NOAA. Version 4 DMSP-OLS Nighttime Lights Time Series. Available online: <http://ngdc.noaa.gov/eog/dmsp/downloadV4composites.html> (accessed on 14 April 2019).
42. Pcfruit. Het Proefcentrum Fruitteelt. Available online: <https://www.pcfruit.be/nl> (accessed on 14 April 2019).
43. Petrić, M. Modelling the Influence of Meteorological Conditions on Mosquito Vector Population Dynamics (Diptera, Culicidae). Ph.D. Thesis, University of Gent and University of Novi Sad, Novi Sad, Serbia, Unpublished.
44. ECMWF. Copernicus Climate Change Service (C3S) (2017): ERA5: Fifth Generation of ECMWF Atmospheric Reanalyses of the Global Climate. Copernicus Climate Change Service Climate Data Store (CDS). Available online: <https://cds.climate.copernicus.eu/cdsapp#!/home> (accessed on 14 April 2019).
45. European Centre for Disease Prevention and Control. Technical Report 2009: Development of Aedes albopictus Risk Maps. Available online: https://ecdc.europa.eu/sites/portal/files/media/en/publications/Publications/0905_TER_Development_of_Aedes_Alboipictus_Risk_Maps.pdf (accessed on 14 April 2019).
46. Fischer, D.; Thomas, S.M.; Niemitz, F.; Reineking, B.; Beierkuhnlein, C. Projection of climatic suitability for Aedes albopictus Skuse (Culicidae) in Europe under climate change conditions. *Glob. Planet. Chang.* **2011**, *78*, 54–64. [[CrossRef](#)]
47. Caminade, C.; Medlock, J.M.; Ducheyne, E.; McIntyre, K.M.; Leach, S.; Baylis, M.; Morse, A.P. Suitability of European climate for the Asian tiger mosquito Aedes albopictus: recent trends and future scenarios. *J. R. Soc. Interface* **2012**, *9*, 2708–2717. [[CrossRef](#)]
48. Institute of Tropical Medicine, Antwerp. New Sightings of Tiger Mosquitoes in Belgium. Available online: <https://www.itg.be/E/Article/new-sightings-of-tiger-mosquito-in-belgium> (accessed on 14 April 2019).
49. Deblauwe, I.; Demeulemeester, J.; De Witte, J.; Hendy, A.; Sohler, C.; Madder, M. Increased detection of Aedes albopictus in Belgium: no overwintering yet, but an intervention strategy is still lacking. *Parasitol. Res.* **2015**, *114*, 3469–3477. [[CrossRef](#)]
50. Medlock, J.M.; Avenell, D.; Barrass, I.; Leach, S. Analysis of the potential for survival and seasonal activity of Aedes albopictus (Diptera: Culicidae) in the United Kingdom. *J. Vector Ecol.* **2006**, *31*, 292–305. [[CrossRef](#)]

51. Meehl, G.A.; Zwiers, F.; Evans, J.; Knutson, T.; Mearns, L.; Whetton, P. Trends in extreme weather and climate events: Issues related to modeling extremes in projections of future climate change. *Bull. Am. Meteorol. Soc.* **2000**, *81*, 427–436. [[CrossRef](#)]
52. Kunkel, K.E.; Pielke, R.A., Jr.; Changnon, S.A. Temporal fluctuations in weather and climate extremes that cause economic and human health impacts: A review. *Bull. Am. Meteorol. Soc.* **1999**, *80*, 1077–1098. [[CrossRef](#)]



© 2019 by the authors. Licensee MDPI, Basel, Switzerland. This article is an open access article distributed under the terms and conditions of the Creative Commons Attribution (CC BY) license (<http://creativecommons.org/licenses/by/4.0/>).